# The Warming Tibetan Plateau improves winter air quality in the Sichuan Basin, China

Shuyu Zhao[1], Tian Feng[2], Xuexi Tie[1,3*], Zebin Wang[4]

[1]Key Laboratory of Aerosol Chemistry and Physics, SKLLQG, Institute of Earth Environment, Chinese Academy of Sciences, Xi'an, 710061, China

[2]Department of Geography & Spatial Information Techniques, Ningbo University, Ningbo, 315211, China

[3]Center for Excellence in Urban Atmospheric Environment, Institute of Urban Environment, Chinese Academy of Sciences, Xiamen, 361021, China

[4]Northwest Air Traffic Management Bureau, Civil Aviation Administration of China, Xi'an, 712000, China

Corresponding author: tiexx@ieecas.cn

## Key points

The Tibetan Plateau is rapidly warming, and the temperature has risen by 2 ° C from 2013 to 2017.

The 2 ° C warming of the plateau leads to an increase in PBL height and a decrease in humidity in the Sichuan Basin.

The 2 ° C warming reduces $PM_{2.5}$ concentration in the basin by 25.1 μg $m^{-3}$, of which primary and secondary aerosols are 5.4 μg $m^{-3}$ and 19.7 μg $m^{-3}$, respectively.

## Abstract

Impacts of global climate change on the occurrence and development of air pollution have attracted more attentions. This study investigates impacts of the warming Tibetan Plateau on air quality in the Sichuan Basin. Meteorological observations and ERA-interim reanalysis data reveal that the Tibetan Plateau has been rapidly warming during the last 40 years (1979-2017), particularly in winter when the warming rate is approximately twice as much as the annual warming rate. Since 2013, the winter temperature over the plateau has even risen by 2 ° C. Here, we use the WRF-CHEM model to assess the impact of the 2 ° C warming on air quality in the Sichuan Basin. The model results show that the 2 ° C warming causes an increase in the Planetary Boundary Layer (PBL) height and a decrease in the relative humidity (RH) in the basin. The elevated PBL height strengthens vertical diffusion of $PM_{2.5}$, while the decreased RH significantly reduces secondary aerosol formation. Overall, $PM_{2.5}$ concentration is reduced by 17.5% (~25.1 μg $m^{-3}$), of which the reduction in primary and secondary aerosols is 5.4 μg $m^{-3}$ and 19.7 μg $m^{-3}$, respectively. These results reveal that the recent warming plateau has improved air quality in the basin, to some certain extent, mitigating the air pollution therein. Nevertheless, climate system is particularly complicated, and more studies are needed to demonstrate the impact of climate change on air quality in the downstream regions as the plateau is likely to continue warming.



**Keywords:** climate change, air quality, Tibetan Plateau, WRF-CHEM model

## 1 Introduction

The Tibetan Plateau is known as the third pole because of its high altitude and large area. It is also regarded as an important response region to the Northern Hemisphere, and even global climate due to its sensitivity to climate change. Previous studies on the Tibetan Plateau show that the region was experiencing warming in the second half of the $20^{th}$ century, especially in the winter months (Kuang and Jiao, 2016; Liu and Chen, 2000; Rangwala et al., 2009). The warming plateau not only plays a significant role in driving the weather and climate change, as well as the ecological system, but also has an important impact on air quality in the downstream regions. Xu et al. (2016) suggest that the thermal anomaly over the Tibetan Plateau obviously increases haze frequency and surface aerosol concentration in central-eastern China.

However, the impacts of climate change on air quality in China are still unclear. Some researches hold the opinion that climate change induced by greenhouse gas emission increases severe haze occurrence and intensity in winter at Beijing, and its impact will continue in the future (Cai et al., 2017; Zou et al., 2017). Similarly, Xu et al. (2017) suggest that climate warming anomaly in the lower and middle troposphere over the continent around the Yangtze River Delta leads to more haze days in winter during recent decades. On the contrary, another opinion suggests that climate change in the past two decades is favorable for air pollution dispersion in northern China via enhancing mid-latitude cold surges in winter (Zhao et al., 2018). If cold surge is strong enough, pollutants would be transported to the downstream regions, causing a better air quality in the upstream region but a worse one in the downstream region. Thus, there may be regional differences in the impact of climate change on air quality.

Previous studies on air pollution in China are concentrated in the developed regions, such as the North China Plain, the Yangtze River Delta and the Pearl River Delta. Few studies have paid attention to the Sichuan Basin, although the region is undergoing severe air pollution, and mean $PM_{2.5}$ concentration is more than 110 μg $m^{-3}$ in winter (Qiao et al., 2019; Tao et al., 2017; Wang et

al., 2018; Yang et al., 2011). Thus, it is necessary to explore the underlying causes that leads to air pollution in the Sichuan Basin.

The Sichuan Basin locates in the downstream region of the Tibetan Plateau, and its weather conditions are obviously affected by the plateau (Duan et al., 2012; Hua, 2017; Zhao et al., 2019). For instance, the foggy weather, southwest vortex and low-level shear line over the basin are closely associated with the plateau (Zhu et al., 2000). These changes in weather conditions induced by the plateau undoubtedly affect the development and dispersion of air pollution in the basin, because the huge terrain can trigger a thermodynamic forcing, which is of great importance for weather conditions in the surrounding regions (Bei et al., 2016; 2017; Zhao et al., 2015).

This study therefore focuses on how climate change on the Tibetan Plateau affects air quality in the Sichuan Basin in recent years. Section 3 analyzes the climate change on the Tibetan Plateau in the past four decades, and especially emphasizes the change in recent five years. In Section 4, we design two numerical simulations to calculate the impact of climate change on air quality. One is a baseline simulation, which is constrained by observed surface meteorological parameters and pollutant concentrations. The other is a sensitivity simulation, which uses the same emission inventory and meteorological fields as the baseline simulation except for the changed air temperature. We compare the difference of $PM_{2.5}$ concentrations in these two cases, and also calculate the differences in meteorological parameters that include winds (wind speed and direction), air temperature, and relative humidity (RH), as well as the Planetary Boundary Layer (PBL) height. Based on the differences in $PM_{2.5}$ concentration and meteorological parameters above, we finally explain the cause-to-effect relationship between climate change on the Tibetan Plateau and the changes in the PBL height and RH in the Sichuan Basin. Moreover, we calculate the effect of the relationship on air quality in the Sichuan Basin.

## 2 Data and Methods

## 2.1 Observations

To ensure a robust result, we use two datasets of surface air temperature in this study. One is the European Center for Medium-Range Weather Forecasts (ECMWF) ERA-Interim monthly mean reanalysis data (1979-2018), obtained from the website of http://apps.ecmwf.int/datasets/, with the finest horizontal resolution of 0.125°×0.125°. The other is hourly and monthly mean weather-station observations from the National Oceanic and Atmospheric Administration (NOAA), which is available on the website of http://gis.ncdc.noaa.gov/map/viewer/#app=clim&cfg=cdo&theme=hourly&layers=1&node=gis.

Figure 1 shows the distribution of weather stations over the Tibetan Plateau, and these weather stations widely cover the entire plateau. Trends of annual mean and winter surface air temperature over the plateau are analyzed, and the winter is averaged over 3-month periods (December-January-February). Additionally, we use ambient air quality data to validate the model performance. Since 2013, the data are released by Ministry of Environmental Protection, China at http://www.aqistudy.cn/, including hourly $PM_{2.5}$, CO, and $O_3$ mass concentrations. The monitoring stations for air quality are also shown in Figure 1.

## 2.2 Model configuration and experiments

A state-of-the-art regional dynamical and chemical model (WRF-CHEM model) is used in the study. The simulation domain covers the Tibetan Plateau and the Sichuan Basin (Figure 1). The Tibetan Plateau covers about 2.5 million $km^2$, with the averaged elevation of 4500 m, and the Sichuan Basin covers about 0.16 million $km^2$, with the elevation in the center of the basin less than 1000 m (250 - 700 m). The model is set by a horizontal grid resolution of 9 km (451 × 221 grids), with 35 vertical sigma levels. The model description in detail is seen by Grell et al. (2005). The evaluation of the model performance has been conducted by many previous studies (Li et al., 2011a; Tie et al., 2009; 2007). In this study, we use the Goddard longwave and shortwave radiation

parameterization (Dudhia, 1989), the WSM 6-class graupel microphysics scheme (Hong and Lim, 2006), the Mellor-Yamada-Janji (MYJ) planetary boundary layer scheme (Janjić, 2002), the unified Noah land-surface model (Chen and Dudhia, 2001) and Monin-Obukhov surface layer scheme (Janjić, 2002). For chemical schemes, we use a new flexible gas-phase chemical module and the Community Multiscale Air Quality (CMAQ, version 4.6) aerosol module developed by the US EPA (Binkowski, 2003). Gas-phase atmospheric reactions of volatile organic compounds (VOCs) and nitrogen oxide (NOx) use the SAPRC-99 (Statewide Air Pollution Research Center, version 1999) chemical mechanism. Inorganic aerosols use the ISORROPIA version 1.7, referring to Li et al. (2011a) and Feng et al. (2016). A $SO_2$ heterogeneous reaction mechanism on aerosol surfaces involving aerosol water is added (Li et al., 2017a), and $NO_2$ heterogeneous reaction to produce HONO is also considered (Li et al., 2010). The secondary organic aerosol (SOA) calculation uses a non-traditional volatility basis-set approach by Li et al. (2011b). The photolysis rates are calculated by a fast Tropospheric Ultraviolet and Visible (FTUV) radiation transfer model, in which the impacts of aerosols and clouds on the photochemistry processes are considered (Li et al., 2011a; Tie et al., 2003; 2005). The wet deposition is calculated by the method used in CMAQ and the dry deposition follows Wesely (1989).

We use the MIX anthropogenic emission inventory for the year of 2010, and it is available at Multi-resolution Emission Inventory for China (http://www.meicmodel.org/dataset-mix.html), consisting of industrial, power, transportation, and agricultural as well as residential sources (Li et al., 2017b; Zhang et al., 2009). The emission inventory is constructed by a 'bottom-up' approach based on national and provincial activity data and emission factors. To improve the emission inventory accuracy, we use a 'top-down' method here to constrain the emission inventory. We compare the simulated value with the measured value time and again until the simulations are close to the measurements. The biogenic emissions are online calculated by the Model of Emissions of Gases and Aerosol from Nature (MEGAN) (Guenther et al., 2006). Initial and boundary meteorological fields in the model are driven by 6-hour 1° × 1° NCEP (National Centers for Environmental Prediction) reanalysis data. Chemical lateral conditions are provided by a global

chemistry transport model – MOZART (Model for OZone And Related chemical Tracer, version 4), with a 6-h output (Emmons et al., 2010; Tie et al., 2005). The spin-up time of the WRF-CHEM model is 1 day.

Two numerical experiments are performed. One is the baseline simulation in the 2013-2014 winter (January 2014), and the other is a sensitivity simulation that has an observational increase in air temperature over the Tibetan Plateau. In other words, the sensitivity simulation uses the same emission inventory and meteorological conditions as the baseline simulation except that the temperature fields over the Tibetan Plateau are changed. According to the meteorological records at weather stations, surface air temperature risen by an average of 2°C from 2013 to 2017 over the Tibetan Plateau (Table S1). ERA-interim reanalysis data also show that the troposphere (600hPa - 250hPa) over the plateau is warming during the 2013-2017 period, and the temperature increment shows a parabolic pattern with the altitude, by an average increase of ~2°C (Figure S1). Thus, we design a sensitivity simulation, with a temperature increase of 2°C in the troposphere over the plateau. In the model, we set to the 2°C warming at all grids covering the plateau (the region surrounded by the dark line in Figure 1b) in the initial and boundary fields. In order to ensure a persistent influence of the 2°C warming, we drive the initial field with a 2°C increment every day. Then, by comparing the difference between the sensitivity simulation and the baseline simulation, we determine the impact of the 2°C warming over the Tibetan Plateau on air quality in the Sichuan Basin.

## 3 The warming Tibetan Plateau in the last four decades

Figure 2 shows the variability and linear trend of surface air temperature at 10 weather stations over the Tibetan Plateau in winter during the last four decades (1979 - 2017). The winter mean temperature recorded from all the weather stations exhibits an obvious annual fluctuation and the linear regression shows a significant rising trend. Clearly, the plateau is continuously undergoing a warming phase, albeit with regional differences in the warming magnitude. The warming rates

187 in different regions vary in the range of 0.5 - 1.0°C decade$^{-1}$. Compared with the warming rate of
188 annual mean temperature (Figure S1), the warming rate in winter is approximately twice as much,
189 suggesting that the warming in winter is more significant.
190
191 Using the ERA-interim reanalysis data, Figure 3 shows the temperature change during the same
192 period (1979 - 2017). The result is consistent with weather records, showing that air temperature
193 is significantly rising in most parts of the plateau. The maximal warming rate is around 0.6 - 0.8°C
194 decade$^{-1}$, appeared in the central and southern plateau. The warming in the rest areas is slighter,
195 with a rate of 0.3 - 0.6 °C decade$^{-1}$. Particularly, the averaged warming rate in the vast central
196 plateau reaches about 1.0°C yr$^{-1}$ in recent five years (Figure S2), greater than the warming rate
197 during the entire 40 years (Figure 3). Both the observation records and reanalysis data evidently
198 show that the plateau has been warming in the last four decades, and also the warming trend for
199 recent years is more significant.
200
201 From the above temperature change analysis, we notice that there is obviously a positive
202 temperature anomaly between 2013 and 2017 winters, implying for an accelerating warming over
203 the plateau. The observational temperature in winter increases by about 2°C between 2013 and
204 2017. Therefore, the impact of the 2°C warming on air quality in the Sichuan Basin is investigated.
205 In order to isolatedly assess the effect of a rapid temperature increase and to eliminate the effect of
206 other factors, a sensitivity study using the WRF-CHEM model is conducted for considering the
207 2°C temperature increase from the value in 2013 (see Figure 2 and Table S1).
208
209 # 4 Results and Discussion
210
211 ## 4.1 Model validation
212
213 To systemically evaluate the model performance on simulation $O_3$, CO and $PM_{2.5}$ mass
214 concentrations, three statistical indices are used. They are the mean bias (MB), root mean square

error (RMSE), and index of agreement (IOA). The calculation formulas are given in Text S1. The IOAs of air temperature and RH are 0.85 and 0.79, respectively (Figure S3), suggesting that the model well captures the diurnal cycle of temperature and the variability of RH. However, the calculated wind speed is overestimated, especially in the region between the Tibetan Plateau and the Sichuan Basin. This is because there is a dramatic elevation drop in the region, which makes it difficult for the model to replicate the observed wind speed and direction.

Figure 4 shows comparisons of hourly $O_3$, CO and $PM_{2.5}$ concentrations between the model simulations and measurements. The result shows that the simulated CO mean level is close to the measurement, with a MB of 0.11 mg $m^{-3}$, indicating that the model reasonably reproduces the meteorological fields and long-range transport. Because the chemical lifetime of CO is relatively long (~months), the variability of CO is dominantly determined by the meteorological fields and atmospheric transport process. For the simulation of $O_3$, in addition to the effects of meteorological fields and atmospheric transport process, its variability is strongly controlled by the photochemical process. The model result shows that the simulated diurnal cycle of $O_3$ is reasonably agreed with the measurement, with an IOA of 0.79. There is only a small bias between the simulated and measured $O_3$ mean concentration. The simulated $O_3$ concentration is 1.7 μg $m^{-3}$ higher than the measurement, suggesting that both the photochemistry and long-range transport well capture the $O_3$ variability in the region. Finally, the IOA between the simulated and measured $PM_{2.5}$ concentrations is 0.80, indicating that the aerosol module in the model generally captures the measured $PM_{2.5}$ variation.

However, there are some noticeable discrepancies between the simulations and the measurements. For instance, the simulated magnitude of $PM_{2.5}$ concentration is larger than the measurement, and its mean level is underestimated by 13.1 μg $m^{-3}$, less than 10% of the measurement (~153.5 μg $m^{-3}$). These discrepancies are likely due to the biases in the uncertainties in emission inventory and small-scale dynamical fields. During the period of Jan 17$^{th}$ to Jan 20$^{th}$, the observed wind speed concentrates in the range of 1 - 2 m $s^{-1}$, with an average of 1.3 m $s^{-1}$, while the simulated wind speed

is obviously higher, with an average of 2.0 m $s^{-1}$ (Figure S3). The observed prevailing wind is northerly wind while the simulated prevails easterly wind. Figure S6a shows that $PM_{2.5}$ concentration is lower in the north to the Sichuan Basin while higher to in the east to the basin. Therefore, the overestimated $PM_{2.5}$ concentration is mainly caused by the departure of winds, which results in a false transport from the east to the basin. This is also shown by the overestimation of CO concentration because the observed northerly wind is not well simulated due to the complicated topography.

### 4.2 Change in winter $PM_{2.5}$ concentration over the basin

To examine impacts of the warming plateau on $PM_{2.5}$ concentration in winter in the Sichuan Basin, the time series of $PM_{2.5}$ concentrations in the two case simulations (i.e., with and without the 2°C warming over the plateau) are respectively calculated (Figure 5). The results show that $PM_{2.5}$ concentration in the basin is significantly reduced by an average of 25.1 μg $m^{-3}$ in the case of 2°C warming, with a confidence level of 99.9% ($p < 0.001$). The maximum hourly reduction reaches to 84.6 μg $m^{-3}$ (Figure S4a) and the maximum percentage reduction is about 64.5% (Figure S4b). Interestingly, the maximum reduction always occurs while $PM_{2.5}$ concentration reaches a peak value, which suggests that the impact of the warming plateau is extremely significant during the period of high $PM_{2.5}$ concentration. This result is similar to previous studies which also point out that extreme weather plays important roles in affecting air quality (De Sario et al., 2013; Hong et al., 2019; Tsangari et al., 2016; Zhang et al., 2016). That is to say, the impact of the warming plateau on air quality is apt to be amplified in extremely high $PM_{2.5}$ concentrations.

To better understand the impact of the warming plateau on $PM_{2.5}$ concentration in the Sichuan Basin, we also calculate the changes in $PM_{2.5}$ chemical composition in the basin (Figure 6). As a result, secondary aerosol reduces by 19.7 μg $m^{-3}$, accounting for 78.5% of the total reduction. For example, the largest reduction is SOA, reducing from 23.2 μg $m^{-3}$ in the base case to 10.8 μg $m^{-3}$ in the warming case. The second reduction is sulfate (31.8 μg $m^{-3}$ in the base case and 28.6 μg $m^{-3}$

in the warming case). The next are nitrate and ammonium (22.3 μg $m^{-3}$ and 19.1 μg $m^{-3}$ in the base case, and 20.2 μg $m^{-3}$ and 17.5 μg $m^{-3}$ in the warming case). Significance testing of the difference in every chemical composition between the baseline and sensitivity simulations are also given in Table S2. The *p*-values of most chemical composition in $PM_{2.5}$ are far less than 0.001 except that the *p*-value of EC is 0.0011 (Table S2), implying for an extremely significant reduction of every chemical composition in $PM_{2.5}$ within the basin when the plateau warms by 2°C.

There are also significant changes in the spatial distribution of $PM_{2.5}$ concentration. Figure 7 shows the spatial distribution of changes in surface $PM_{2.5}$ concentration and winds after 2°C warming over the plateau. Apparently, there is a larger decrease in $PM_{2.5}$ concentration in the whole basin, and the maximum reduction is more than 30 μg $m^{-3}$. By contrast, $PM_{2.5}$ concentration increases by 5 - 15 μg $m^{-3}$ at the eastern edge of the plateau. Wind patterns show that easterly winds over the basin enhance while westerly wind over the plateau weaken (Figure S6 and Figure 7). We further compare the difference in the surface pressure between the baseline and sensitivity simulations, and find out that surface pressure over the plateau and the basin all decreases when the plateau warms by 2°C (Figure 8a and 8b). Over the plateau, the pressure drop has a decrease characteristic from west to east (Figure 8c), which results in a decreased pressure gradient and a weakened westerly wind. While in the basin, the pressure drop is less than the plateau. This leads to an increased pressure gradient from the basin to the plateau, inducing an intensified easterly wind. The enhanced easterly wind causes an increased transport of $PM_{2.5}$ from the basin to the plateau. On the other hand, the weakened westerly wind and the enhanced easterly wind are convergent at the border between the plateau and the basin (Figure 7), jointly leading to an increase in $PM_{2.5}$ concentration at the eastern edge of the plateau. Additionally, northerly winds over the basin slightly enhance, conducive to diluting the air and reducing $PM_{2.5}$ concentration. Both easterly winds transport and northerly winds dilution are favorable for a reduction of $PM_{2.5}$ concentration in the basin. In addition to the wind effect, there are also other important factors to produce the $PM_{2.5}$ reduction in the basin, such as the PBL height and RH, which will be analyzed as follows.

### 4.3 Impact of PBL height on $PM_{2.5}$ concentration

Previous studies show that the PBL development plays an important role in diffusing pollutants (Miao et al., 2017; Su et al., 2018; Tie et al., 2015). Here we calculate the change in the PBL height due to the 2°C warming over the plateau, and then analyze the effect of the change in PBL height on $PM_{2.5}$ concentration in the basin.

Our results suggest that the 2°C warming plays different roles in the PBL development over the plateau and the basin. Due to the 2°C warming, the PBL height decreases in most areas of the plateau, but rises by 50 - 200 m over the basin (Figure 9). As known, a shallow PBL constrains $PM_{2.5}$ near the surface via suppressing vertical dispersion (Fan et al., 2011; Iversen, 1984). Conversely, a deep PBL is favorable for $PM_{2.5}$ diffusion. Thus, we explore the underlying cause that leads to the difference in the PBL height over the plateau and the basin. Figure 10 shows that vertical profiles of changes in temperature and winds in the plateau and the basin, because the PBL height is strongly related to the changes in vertical temperature and wind. The results show that the 2°C warming causes a maximum warm layer around 1 km above the ground of the plateau. Interestingly, the warm layer acts as a dome covering 4.5 km above the Sichuan Basin (Figure 10a). Xu et al. (2017) also finds out a significant warm plume extending from the plateau to the downstream Sichuan Basin and Yangtze River Delta by use of NCEP/NCAR reanalysis data. This is probably due to a sharp topography decrease (from ~ 5 km in the plateau to < 1 km in the basin) that leads to a warm plume via subsidence. In the basin, there is a decrease in the temperature from the surface to ~ 4 km, with a maximal temperature reduction (1 - 2°C) located at 1.5 km to 3 km above the ground (Figure 10a). We speculate that changes in the surface pressure can account for the maximal temperature reduction here. After the 2°C warming, surface pressure decreases in the basin (Figure 8), which produces more convergent airflow (as shown in Figure 7). The strengthened convergent airflow induces an intensified ascending motion, conducive to a reduction of temperature in the basin. As a result, the zone where the maximal temperature drop appears, overlaps with the zone with the maximal ascending motion. Furthermore, the intensified updraft increases the vertical temperature

gradient and the instability in the lower troposphere of the basin, thereby causing a higher PBL height than that in the non-warming case (Figure 10b). On the contrary, the change in vertical temperature profile leads to a decreased vertical temperature gradient and increased thermal stability in the lower troposphere of the plateau, in which the PBL height decreases.

On the other hand, the convergent airflows by a weakened westerly wind over the plateau and a strengthened easterly wind in the basin (shown in Figure 8) triggers an ascending motion on the east side of the plateau, which is also beneficial to the development of the PBL height in the basin. Consequently, the elevated PBL facilitates vertical diffusion, leading to a reduction in $PM_{2.5}$ concentration over the basin.

### 4.4 Effect of RH on $PM_{2.5}$ concentration

In addition to the PBL height, ambient RH is a key factor for secondary aerosol formation (Tie et al., 2017; Wang et al., 2016). Previous studies indicate that aerosol hygroscopic growth cannot occurs until the humidity exceeds 50% (Liu et al., 2008). When the humidity is greater than 60%, hygroscopic growth factor of urban aerosol increases significantly with humidity (Liu et al., 2008).

Figure 11 shows that there is remarkable change in RH in the basin due to the 2°C warming of the plateau. In the baseline simulation, the RH varies in the range of 40% - 80% over the basin (Figure 11a). However, the RH varies from 40% to 70% in the 2 °C warming simulation (Figure 11b), suggesting that the basin becomes drier when the plateau is warmer.

The RH comparison between these two numerical simulations reveals that the 2 °C warming causes a 2.5% - 10% decrease in the RH over the basin (Figure 11c). This change in RH has a critical effect on the secondary aerosol formation. As explained by Tie et al. (2017), the reduction of RH (especially during the stage of RH from 80% to 70%) causes a significant decrease of hygroscopic growth on the aerosol surface, resulting in less water surface for producing secondary aerosol, such as sulfate and nitrate. As a result, the $PM_{2.5}$ concentration decreases in the basin. There are also some

fingerprints of the RH's effect on $PM_{2.5}$ concentration. Firstly, the spatial distributions of RH reduction and $PM_{2.5}$ concentration reduction have similar patterns (Figure 11c and Figure 7), and the region with more humidity decrease overlaps the region with more $PM_{2.5}$ decreases. Secondly, as shown in Figure 6, the changes in $PM_{2.5}$ compositions indicate that the reduced $PM_{2.5}$ concentration is mainly caused by the decrease in secondary aerosol concentration. Therefore, the RH change plays an important role for $PM_{2.5}$ concentration in the basin.

## 5 Conclusions

ERA-interim reanalysis data and observation records at 10 weather stations show that the Tibetan Plateau is significantly warming during the past four decades (1979-2017), particularly in winter. The temperature increase rate is 0.5°C decade$^{-1}$ to 1.0°C decade$^{-1}$ in winter, approximately twice as much as the increase rate of annual mean temperature. In recent 5 years (2013-2017), the central plateau is significantly warming with an increase rate of 1.0°C yr$^{-1}$, encompassing the warming rate during the entire 40 years. Rapid warming has caused the winter temperature to increase by an average of 2°C over the entire plateau from 2013 to 2017.

The WRF-Chem model is used to assess the impact of 2°C warming of the plateau on air quality over the downstream Sichuan Basin. The most significant impact of the 2°C warming on $PM_{2.5}$ concentration in the basin is via reducing relative humidity and increasing PBL height. A lower ambient humidity decreases aerosol hygroscopic growth, which weakens secondary aerosol formation and leads to a significant reduction in secondary aerosol concentration. Moreover, the 2°C warming induces an increase in vertical temperature gradient over the basin, strengthening turbulence mixing and elevating PBL height. The elevated PBL height is favorable for vertical diffusion that causes a reduction of $PM_{2.5}$ in the basin. Additionally, the uplift effect by an enhanced ascending motion at the eastern edge of the plateau also contributes to $PM_{2.5}$ reduction within the basin.

In summary, the 2°C warming over the plateau in recent five years comprehensively induces a rising PBL height and a drying ambient air over the basin, which greatly reduces $PM_{2.5}$ secondary compositions. On average, $PM_{2.5}$ concentration reduces by 25.1 μg $m^{-3}$, of which the primary and secondary aerosols decrease by 5.4 μg $m^{-3}$ and 19.7 μg $m^{-3}$, respectively. Since the plateau is likely to continue warming, in-depth understanding to climate change on the Tibetan Plateau is required. Long-term $PM_{2.5}$ monitoring is also needed to validate the impact of the warming plateau on air quality.

*Data availability*. The data used in this study are available from the corresponding author upon request (tiexx@ieecas.cn).

*Supplement.* Supplemental materials to this article can be found online at http://xxxxxx

*Author contributions.* XX designed research, and revised the final paper. SY performed research, and wrote the paper. XX and SY provided financial support. TF validated the model, modified the chart code and reviewed the paper. ZB collected and analyzed the weather-stations data.

*Competing interests.* The authors declare that they have no conflict of interest.

*Acknowledgements.* This work is supported by the National Natural Science Foundation of China (Nos. 41430424, 41730108 and 41807307) and the West Light Foundation of the Chinese Academy of Sciences (Nos. XAB2016B04). We also would like to acknowledge European Center for Medium-Range Weather Forecasts (ERA-interim) for reanalysis data which are freely obtained by a following registration on the website http://apps.ecmwf.int/datasets/. Ambient weather-station observations are obtained from the National Oceanic and Atmospheric Administration (NOAA), http://gis.ncdc.noaa.gov/map/viewer/#app=clim&cfg=cdo&theme=hourly&layers=1&node=gis. The hourly ambient surface $O_3$, CO and $PM_{2.5}$ mass concentrations are real-timely released by Ministry of Environmental Protection, China on the website http://www.aqistudy.cn/, freely downloaded from http://106.37.208.233:20035/. The MEIC-2012 (Multi-resolution Emission Inventory for China) anthropogenic emission inventory is available on the website, http://www.meicmodel.org. The authors also thank anonymous reviewers for their helpful comments and suggestions.

## Reference

Bei, N., Li, G., Huang, R.-J., Cao, J., Meng, N., Feng, T., Liu, S., Zhang, T., Zhang, Q. and Molina, L. T.: Typical synoptic situations and their impacts on the wintertime air pollution in the Guanzhong

basin, China, Atmos. Chem. Phys., 16(11), 7373–7387, doi:10.5194/acp-16-7373-2016, 2016.

Bei, N., Zhao, L., Xiao, B., Meng, N. and Feng, T.: Impacts of local circulations on the wintertime air pollution in the Guanzhong Basin, China, Science of The Total Environment, 592, 373–390, doi:10.1016/j.scitotenv.2017.02.151, 2017.

Binkowski, F. S.: Models-3 Community Multiscale Air Quality (CMAQ) model aerosol component 1. Model description, J. Geophys. Res., 108(D6), 2981, doi:10.1029/2001JD001409, 2003.

Cai, W., Li, K., Liao, H., Wang, H. and Wu, L.: Weather conditions conducive to Beijing severe haze more frequent under climate change, Nat. Clim. Change, 7(4), 257–262, doi:10.1038/nclimate3249, 2017.

Chen, F. and Dudhia, J.: Coupling an Advanced Land Surface–Hydrology Model with the Penn State–NCAR MM5 Modeling System. Part I: Model Implementation and Sensitivity, Mon. Weather Rev., 129(4), 569–585, doi:10.1175/1520-0493(2001)129<0569:CAALSH>2.0.CO;2, 2001.

De Sario, M., Katsouyanni, K. and Michelozzi, P.: Climate change, extreme weather events, air pollution and respiratory health in Europe, Eur Respir J, 42(3), 826–843, doi:10.1183/09031936.00074712, 2013.

Duan, A., Wu, G., Liu, Y., Ma, Y. and Zhao, P.: Weather and climate effects of the Tibetan Plateau, Adv. in Atmos. Sci., 29(5), 978–992, doi:10.1007/s00376-012-1220-y, 2012.

Dudhia, J.: Numerical Study of Convection Observed during the Winter Monsoon Experiment Using a Mesoscale Two-Dimensional Model, J. Atmos. Sci., 46(20), 3077–3107, doi:10.1175/1520-0469(1989)046<3077:NSOCOD>2.0.CO;2, 1989.

Emmons, L. K., Walters, S., Hess, P. G., Lamarque, J. F., Pfister, G. G., Fillmore, D., Granier, C., Guenther, A., Kinnison, D., Laepple, T., Orlando, J., Tie, X., Tyndall, G., Wiedinmyer, C., Baughcum, S. L. and Kloster, S.: Description and evaluation of the Model for Ozone and Related chemical Tracers, version 4 (MOZART-4), Geosci. Model Dev., 3(1), 43–67, doi:10.5194/gmd-3-43-2010, 2010.

Fan, S. J., Fan, Q., Yu, W., Luo, X. Y., Wang, B. M., Song, L. L. and Leong, K. L.: Atmospheric boundary layer characteristics over the Pearl River Delta, China, during the summer of 2006: measurement and model results, Atmos. Chem. Phys., 11(13), 6297–6310, doi:10.5194/acp-11-6297-2011, 2011.

Feng, T., Li, G., Cao, J., Bei, N., Shen, Z., Zhou, W., Liu, S., Zhang, T., Wang, Y., Huang, R.-J., Tie, X. and Molina, L. T.: Simulations of organic aerosol concentrations during springtime in the Guanzhong Basin, China, Atmos. Chem. Phys., 16(15), 10045–10061, doi:10.5194/acp-16-10045-2016, 2016.

Grell, G. A., Peckham, S. E., Schmitz, R., McKeen, S. A., Frost, G., Skamarock, W. C. and Eder,

B.: Fully coupled “online” chemistry within the WRF model, Atmos. Environ., 39(37), 6957–6975, doi:10.1016/j.atmosenv.2005.04.027, 2005.

Guenther, A., Karl, T., Harley, P., Wiedinmyer, C., Palmer, P. I. and Geron, C.: Estimates of global terrestrial isoprene emissions using MEGAN (Model of Emissions of Gases and Aerosols from Nature), Atmos. Chem. Phys., 6(11), 3181–3210, doi:10.5194/acp-6-3181-2006, 2006.

Hong, C., Zhang, Q., Zhang, Y., Davis, S. J., Tong, D., Zheng, Y., Liu, Z., Guan, D., He, K. and Schellnhuber, H. J.: Impacts of climate change on future air quality and human health in China, P. Natl. Acad. Sci. USA, 116(35), 17193–17200, doi:10.1073/pnas.1812881116, 2019.

Hong, S.-Y. and Lim, J.-O. J.: The WRF single-moment 6-class microphysics scheme (WSM6), J. Korean Meteor. Soc., 42(2), 129–151, 2006.

Hua, M.: Analysis and simulation study on the influence of heat condition over Qinghai-Xizang Plateau on climate over South-West China, Plateau Meteorology, 22, 152–156, 2017.

Iversen, T.: On the atmospheric transport of pollution to the Arctic, Geophys. Res. Lett., 11(5), 457–460, doi:10.1029/GL011i005p00457, 1984.

Janjić, Z. I.: Nonsingular implementation of the Mellor-Yamada level 2.5 scheme in the NCEP meso model, Camp Springs, MD. 2002.

Kuang, X. and Jiao, J. J.: Review on climate change on the Tibetan Plateau during the last half century, J. Geophys. Res., 1–29, doi:10.1002/(ISSN)2169-8996, 2016.

Li, G., Bei, N., Cao, J., Huang, R., Wu, J., Feng, T., Wang, Y., Liu, S., Zhang, Q., Tie, X. and Molina, L. T.: A possible pathway for rapid growth of sulfate during haze days in China, Atmos. Chem. Phys., 17(5), 3301–3316, doi:10.5194/acp-17-3301-2017, 2017a.

Li, G., Bei, N., Tie, X. and Molina, L. T.: Aerosol effects on the photochemistry in Mexico City during MCMA-2006/MILAGRO campaign, Atmos. Chem. Phys., 11(11), 5169–5182, doi:10.5194/acp-11-5169-2011, 2011a.

Li, G., Lei, W., Zavala, M., Volkamer, R., Dusanter, S., Stevens, P. and Molina, L. T.: Impacts of HONO sources on the photochemistry in Mexico City during the MCMA-2006/MILAGO Campaign, Atmos. Chem. Phys., 10(14), 6551–6567, doi:10.5194/acp-10-6551-2010, 2010.

Li, G., Zavala, M., Lei, W., Tsimpidi, A. P., Karydis, V. A., Pandis, S. N., Canagaratna, M. R. and Molina, L. T.: Simulations of organic aerosol concentrations in Mexico City using the WRF-CHEM model during the MCMA-2006/MILAGRO campaign, Atmos. Chem. Phys., 11(8), 3789–3809, doi:10.5194/acp-11-3789-2011, 2011b.

Li, M., Zhang, Q., Kurokawa, J.-I., Woo, J.-H., He, K., Lu, Z., Ohara, T., Song, Y., Streets, D. G., Carmichael, G. R., Cheng, Y., Hong, C., Huo, H., Jiang, X., Kang, S., Liu, F., Su, H. and Zheng, B.: MIX: a mosaic Asian anthropogenic emission inventory under the international collaboration

framework of the MICS-Asia and HTAP, Atmos. Chem. Phys., 17(2), 935–963, doi:10.5194/acp-17-935-2017, 2017b.

Liu, X. and Chen, B.: CLIMATIC WARMING IN THE TIBETAN PLATEAU DURING RECENT DECADES, Int. J. Climatol., 20, 1729–1742, 2000.

Liu, X., Cheng, Y., Zhang, Y., Jung, J., Sugimoto, N., Chang, S.-Y., Kim, Y. J., Fan, S. and Zeng, L.: Influences of relative humidity and particle chemical composition on aerosol scattering properties during the 2006 PRD campaign, Atmos. Environ., 42(7), 1525–1536, doi:10.1016/j.atmosenv.2007.10.077, 2008.

Miao, Y., Guo, J., Liu, S., Liu, H., Li, Z., Zhang, W. and Zhai, P.: Classification of summertime synoptic patterns in Beijing and their associations with boundary layer structure affecting aerosol pollution, Atmos. Chem. Phys., 17(4), 3097–3110, doi:10.5194/acp-17-3097-2017, 2017.

Qiao, X., Guo, H., Tang, Y., Wang, P., Deng, W., Zhao, X., Hu, J., Ying, Q. and Zhang, H.: Local and regional contributions to fine particulate matter in the 18 cities of Sichuan Basin, southwestern China, Atmos. Chem. Phys., 19(9), 5791–5803, doi:10.5194/acp-19-5791-2019, 2019.

Rangwala, I., Miller, J. R. and Xu, M.: Warming in the Tibetan Plateau: Possible influences of the changes in surface water vapor, Geophys. Res. Lett., 36(6), 5–6, doi:10.1029/2009GL037245, 2009.

Su, T., Li, Z. and Kahn, R.: Relationships between the planetary boundary layer height and surface pollutants derived from lidar observations over China: regional pattern and influencing factors, Atmos. Chem. Phys., 18(21), 15921–15935, doi:10.5194/acp-18-15921-2018, 2018.

Tao, J., Zhang, L., Cao, J. and Zhang, R.: A review of current knowledge concerning PM 2. 5chemical composition, aerosol optical properties and their relationships across China, Atmos. Chem. Phys., 17(15), 9485–9518, doi:10.5194/acp-17-9485-2017, 2017.

Tie, X., Huang, R.-J., Cao, J., Zhang, Q., Cheng, Y., Su, H., Di Chang, schl, U. P. X., Hoffmann, T., Dusek, U., Li, G., Worsnop, D. R. and Dowd, C. D. O. X.: Severe Pollution in China Amplified by Atmospheric Moisture, Sci. Rep., 1–8, doi:10.1038/s41598-017-15909-1, 2017.

Tie, X., Madronich, S., Li, G., Ying, Z., Weinheimer, A., Apel, E. and Campos, T.: Simulation of Mexico City plumes during the MIRAGE-Mex field campaign using the WRF-Chem model, Atmos. Chem. Phys., 9(14), 4621–4638, doi:10.5194/acp-9-4621-2009, 2009.

Tie, X., Madronich, S., Li, G., Ying, Z., Zhang, R., Garcia, A. R., Lee-Taylor, J. and Liu, Y.: Characterizations of chemical oxidants in Mexico City: A regional chemical dynamical model (WRF-Chem) study, Atmos. Environ., 41(9), 1989–2008, doi:10.1016/j.atmosenv.2006.10.053, 2007.

Tie, X., Madronich, S., Walters, S., Zhang, R., Rasch, P. and Collins, W.: Effect of clouds on photolysis and oxidants in the troposphere, J. Geophys. Res., 108(D20), 4642,

518 doi:10.1029/2003JD003659, 2003.

519 Tie, X., Sasha, M., Stacy, W., David, E., Paul, G., Natalie, M., Renyi, Z., Lou, C. and Guy, B.:
520 Assessment of the global impact of aerosols on tropospheric oxidants, J. Geophys. Res.,
521 110(D03204), 13,791, doi:10.1029/2004JD005359, 2005.

522 Tie, X., Zhang, Q., He, H., Cao, J., Han, S., Gao, Y., Li, X. and Jia, X. C.: A budget analysis of the
523 formation of haze in Beijing, Atmos. Environ., 100, 25–36, doi:10.1016/j.atmosenv.2014.10.038,
524 2015.

525 Tsangari, H., Paschalidou, A. K., Kassomenos, A. P., Vardoulakis, S., Heaviside, C., Georgiou, K.
526 E. and Yamasaki, E. N.: Extreme weather and air pollution effects on cardiovascular and respiratory
527 hospital admissions in Cyprus, Science of The Total Environment, 542(Part A), 247–253,
528 doi:10.1016/j.scitotenv.2015.10.106, 2016.

529 Wang, G., Zhang, R., Gomez, M. E., Yang, L., Levy Zamora, M., Hu, M., Lin, Y., Peng, J., Guo,
530 S., Meng, J., Li, J., Cheng, C., Hu, T., Ren, Y., Wang, Y., Gao, J., Cao, J., An, Z., Zhou, W., Li, G.,
531 Wang, J., Tian, P., Marrero-Ortiz, W., Secrest, J., Du, Z., Zheng, J., Shang, D., Zeng, L., Shao, M.,
532 Wang, W., Huang, Y., Wang, Y., Zhu, Y., Li, Y., Hu, J., Pan, B., Cai, L., Cheng, Y., Ji, Y., Zhang,
533 F., Rosenfeld, D., Liss, P. S., Duce, R. A., Kolb, C. E. and Molina, M. J.: Persistent sulfate formation
534 from London Fog to Chinese haze, P. Natl. Acad. Sci. USA, 113(48), 13630–13635,
535 doi:10.1073/pnas.1616540113, 2016.

536 Wang, H., Tian, M., Chen, Y., Shi, G., Liu, Y., Yang, F., Zhang, L., Deng, L., Yu, J., Peng, C. and
537 Cao, X.: Seasonal characteristics, formation mechanisms and source origins of $PM_{2.5}$ in two
538 megacities in Sichuan Basin, China, Atmos. Chem. Phys., 18(2), 865–881, doi:10.5194/acp-18-865-
539 2018, 2018.

540 Wesely, M. L.: Parameterization of surface resistances to gaseous dry deposition in regional-scale
541 numerical models, Atmospheric Environment (1967), 23(6), 1293–1304, doi:10.1016/0004-
542 6981(89)90153-4, 1989.

543 Xu, J., Chang, L., Yan, F. and He, J.: Role of climate anomalies on decadal variation in the
544 occurrence of wintertime haze in the Yangtze River Delta, China, Science of The Total Environment,
545 599-600, 918–925, doi:10.1016/j.scitotenv.2017.05.015, 2017.

546 Xu, X., Zhao, T., Liu, F., Gong, S. L., Kristovich, D., Lu, C., Guo, Y., Cheng, X., Wang, Y. and
547 Ding, G.: Climate modulation of the Tibetan Plateau on haze in China, Atmos. Chem. Phys., 16(3),
548 1365–1375, doi:10.5194/acp-16-1365-2016, 2016.

549 Yang, F., Tan, J., Zhao, Q., Du, Z., He, K., Ma, Y., Duan, F., Chen, G. and Zhao, Q.: Characteristics
550 of PM 2.5speciation in representative megacities and across China, Atmos. Chem. Phys., 11(11),
551 5207–5219, doi:10.5194/acp-11-5207-2011, 2011.

552 Zhang, H., Wang, Y., Park, T.-W. and Deng, Y.: Quantifying the relationship between extreme air

pollution events and extreme weather events, Atmospheric Research, 1–48, doi:10.1016/j.atmosres.2016.11.010, 2016.

Zhang, Q., Streets, D. G., Carmichael, G. R., He, K. B., Huo, H., Kannari, A., Klimont, Z., Park, I. S., Reddy, S., Fu, J. S., Chen, D., Duan, L., Lei, Y., Wang, L. T. and Yao, Z. L.: Asian emissions in 2006 for the NASA INTEX-B mission, Atmos. Chem. Phys., 9(14), 5131–5153, doi:10.5194/acp-9-5131-2009, 2009.

Zhao, P., Li, Y., Guo, X., Xu, X., Liu, Y., Tang, S., Xiao, W., Shi, C., Ma, Y., Yu, X., Liu, H., Jia, L., Chen, Y., Liu, Y., Li, J., Luo, D., Cao, Y., Zheng, X., Chen, J., Xiao, A., Yuan, F., Chen, D., Pang, Y., Hu, Z., Zhang, S., Dong, L., Hu, J., Han, S. and Zhou, X.: The Tibetan Plateau Surface-Atmosphere Coupling System and Its Weather and Climate Effects: The Third Tibetan Plateau Atmospheric Science Experiment, J Meteorol Res, 33(3), 375–399, doi:10.1007/s13351-019-8602-3, 2019.

Zhao, S., Feng, T., Tie, X., Long, X., Li, G., Cao, J., Zhou, W. and An, Z.: Impact of Climate Change on Siberian High and Wintertime Air Pollution in China in Past Two Decades, Earth's Future, 6, 118–133, doi:10.1002/2017EF000682, 2018.

Zhao, S., Tie, X., Cao, J. and Zhang, Q.: Impacts of mountains on black carbon aerosol under different synoptic meteorology conditions in the Guanzhong region, China, Atmospheric Research, 164-165(C), 286–296, doi:10.1016/j.atmosres.2015.05.016, 2015.

Zhu, Q., Shou, S. and Tang, D.: Principles and methods of weather, 4 ed., Beijing. 2000.

Zou, Y., Wang, Y., Zhang, Y. and Koo, J.-H.: Arctic sea ice, Eurasia snow, and extreme winter haze in China, Sci. Adv., 3(3), e1602751–9, doi:10.1126/sciadv.1602751, 2017.

## Figure captions

**Figure 1** (a) Location map of the Tibetan Plateau (the region surrounded by the dark line) and the Sichuan Basin (the region surrounded by the gray line). (b) The model domain and the distribution of weather stations marked in the triangles over the Tibetan Plateau and air quality stations marked in the circles over the Sichuan Basin.

**Figure 2** Trends of observational winter (Dec-Jan-Feb) mean temperature anomaly recorded by 10 weather stations over the Tibetan Plateau during the last four decades (1979-2017).

**Figure 3** Trends of ERA-interim reanalysis winter mean temperature over the Tibetan Plateau from 1979 to 2017. The dotted regions show statistical significance with 95% confidence level ($p$-value < 0.05) from the Student's $t$ test.

**Figure 4** Comparison between the observed (black dots) and simulated (blue line) hourly $O_3$ (μg $m^{-3}$), CO (mg $m^{-3}$) and $PM_{2.5}$ mass concentration (μg $m^{-3}$) over the Sichuan Basin in January 2014.

**Figure 5** Time series of $PM_{2.5}$ concentration over the Sichuan Basin, the baseline simulation is selected in January 2014 and the sensitivity simulation in which 2°C warming occurs over the Tibetan Plateau relative to the baseline simulation.

**Figure 6** Comparison of chemical composition of $PM_{2.5}$ concentration between the baseline simulation (red bar) and sensitivity simulation (blue bar) over the Sichuan Basin.

**Figure 7** Difference in spatial distributions of surface $PM_{2.5}$ concentration (shading) and winds (arrows) between the sensitivity simulation and baseline simulation. The negative shows $PM_{2.5}$ concentration decreases and the positive shows $PM_{2.5}$ concentration increases when the Tibetan Plateau is 2°C warming.

**Figure 8** Comparison of spatial distributions of sea level pressure (SLP) between the (a) baseline simulation and (b) sensitivity simulation over the Tibetan Plateau and Sichuan Basin. (c) The SLPs over the plateau and basin decrease while the plateau becomes 2°C warming.

**Figure 9** Spatial change in the PBL height induced by 2°C warming over the Tibetan Plateau. The positive shows the PBL height increases while the negative shows the PBL height decreases.

**Figure 10** Vertical profiles of changes in temperature (shading and gray contour) and winds (arrows) along 30°N in January 2014. The gray shaded area presents topography. The green box for the Sichuan Basin, and the red solid (baseline simulation) and dash (sensitivity simulation) lines for the PBL height. (a) The Tibetan Plateau and Sichuan Basin, and (b) The Sichuan Basin.

**Figure 11** Comparison of spatial distributions of relative humidity (RH) between the (a) baseline simulation and (b) sensitivity simulation over the Tibetan Plateau and Sichuan Basin. (c) Spatial changes in RH after the plateau becomes 2°C warming, and the positive shows the RH increases while the negative shows the RH decreases.

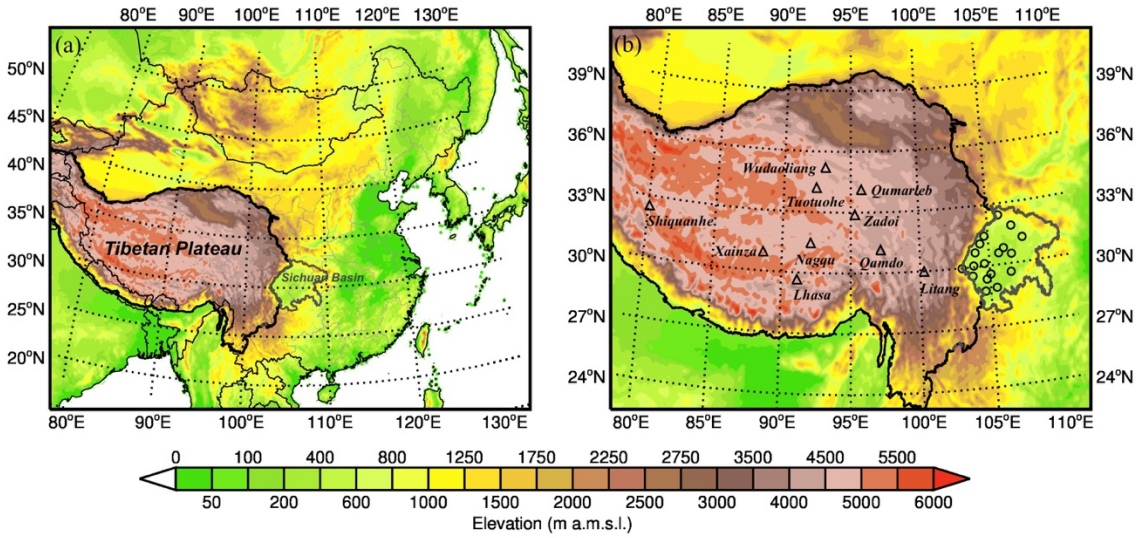


**Figure 1** (a) Location map of the Tibetan Plateau (the region surrounded by the dark line) and the Sichuan Basin (the region surrounded by the gray line). (b) The model domain and the distribution of weather stations marked in the triangles over the Tibetan Plateau and air quality stations marked in the circles over the Sichuan Basin.

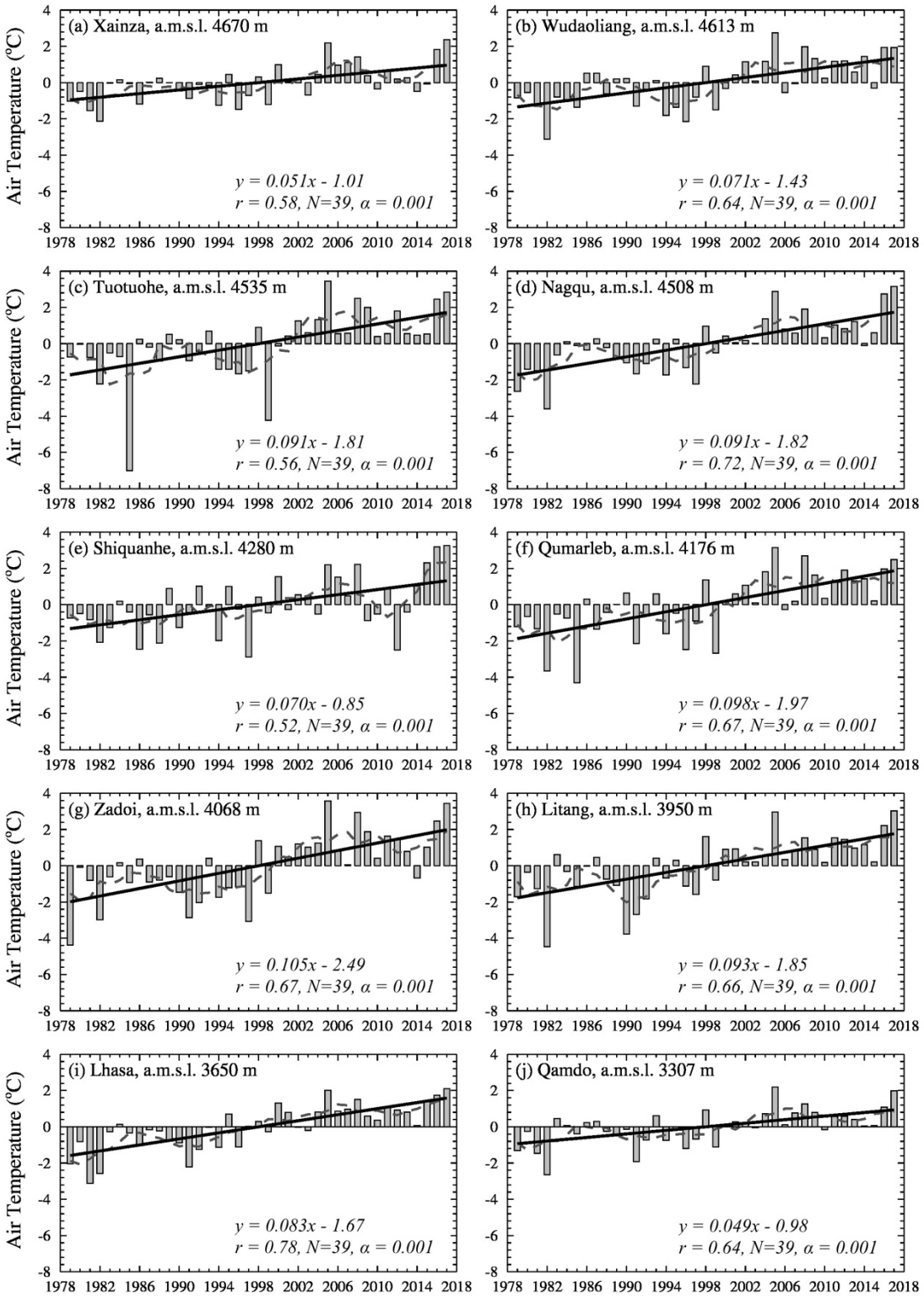


**Figure 2** Trends of observational winter (Dec-Jan-Feb) mean temperature anomaly recorded by 10 weather stations over the Tibetan Plateau during the last four decades (1979-2017).

621

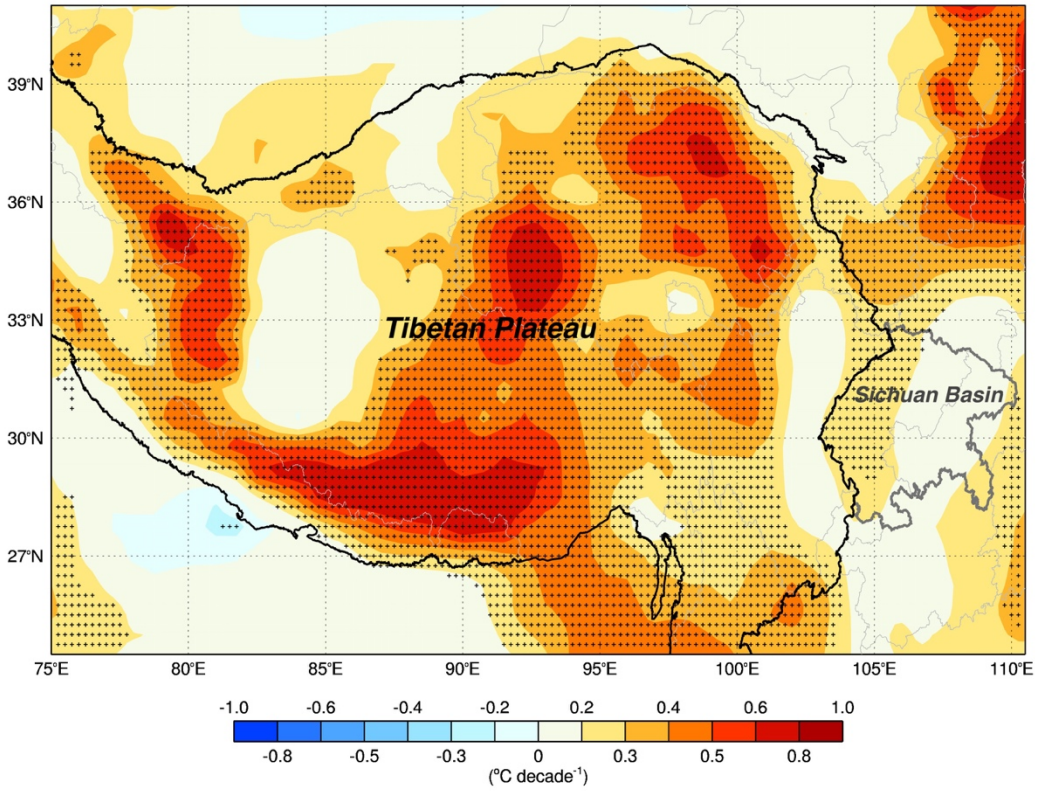


622

623 **Figure 3** Trends of ERA-interim reanalysis winter mean temperature over the Tibetan Plateau from 1979 to
624 2017. The dotted regions show statistical significance with 95% confidence level ($p$-value < 0.05) from the
625 Student's $t$ test.

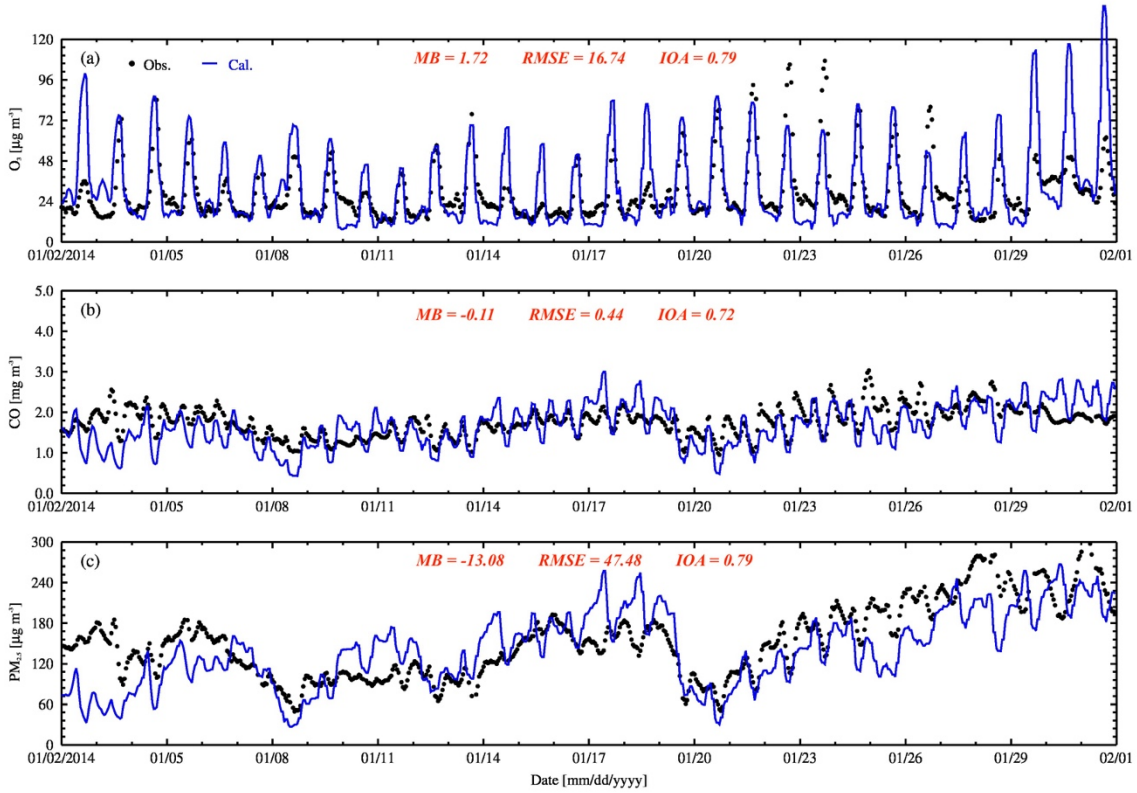


**Figure 4** Comparison between the observed (black dots) and simulated (blue line) hourly $O_3$ (μg $m^{-3}$), CO (mg $m^{-3}$) and $PM_{2.5}$ mass concentration (μg $m^{-3}$) over the Sichuan Basin in January 2014.

631

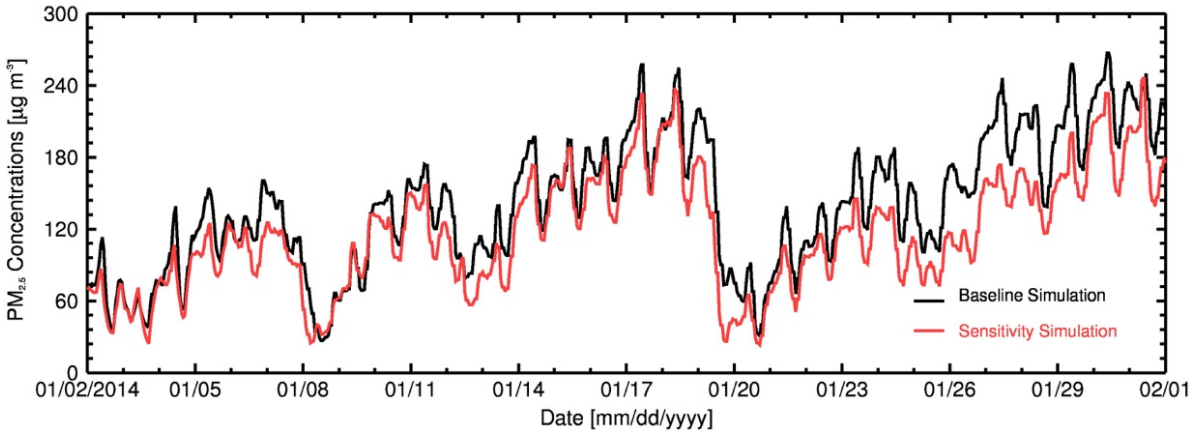


632

633 **Figure 5** Time series of $PM_{2.5}$ concentration over the Sichuan Basin, the baseline simulation is selected in
634 January 2014 and the sensitivity simulation in which 2°C warming occurs over the Tibetan Plateau relative
635 to the baseline simulation.

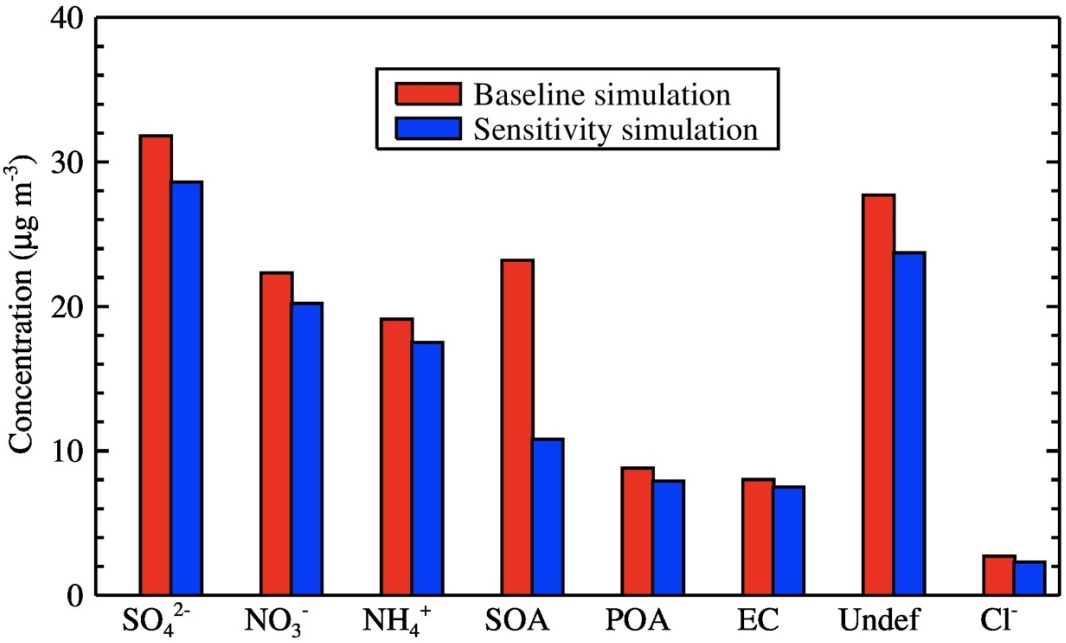


**Figure 6** Comparison of chemical composition of $PM_{2.5}$ concentration between the baseline simulation (red bar) and sensitivity simulation (blue bar) over the Sichuan Basin.

640

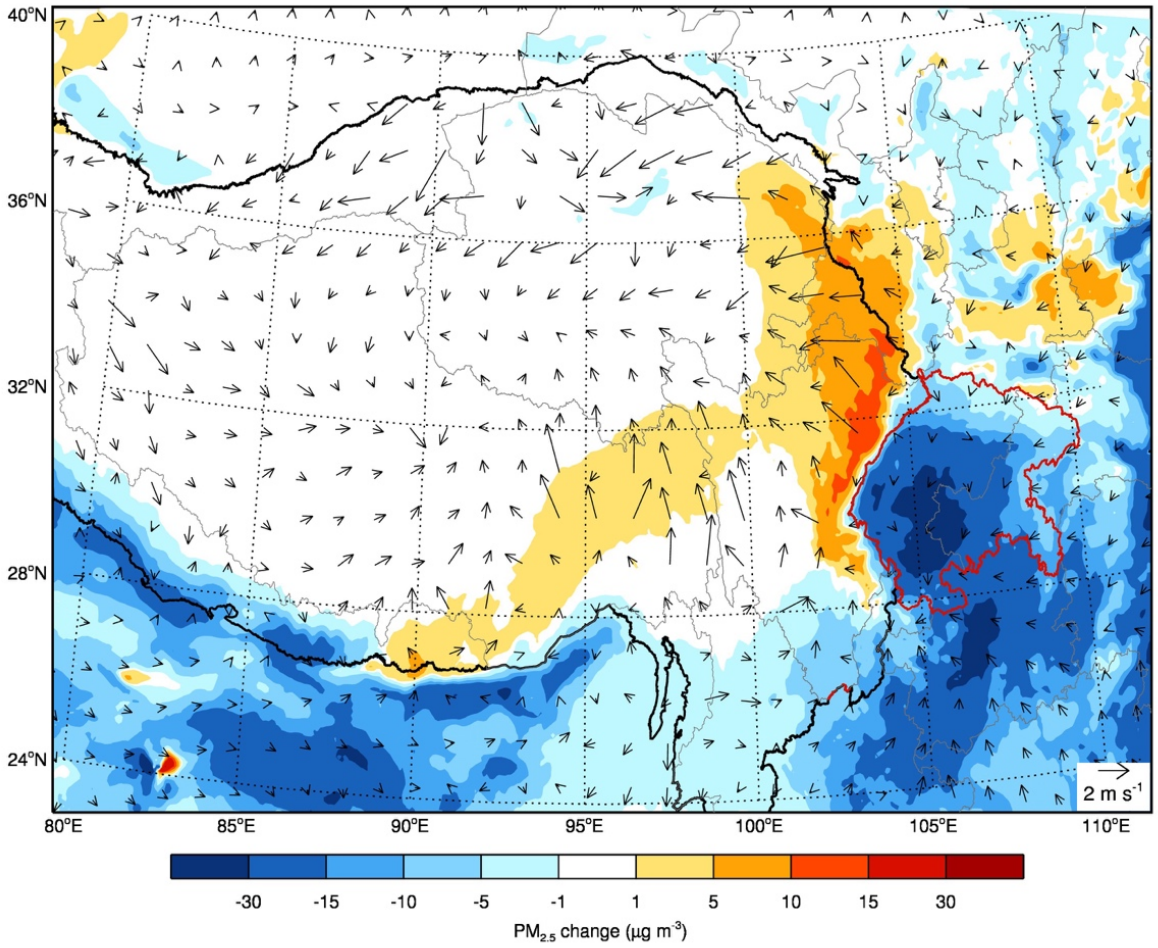


641

642 **Figure 7** Difference in spatial distributions of surface $PM_{2.5}$ concentration (shading) and winds (arrows)
643 between the sensitivity simulation and baseline simulation. The negative shows $PM_{2.5}$ concentration
644 decreases and the positive shows $PM_{2.5}$ concentrations increases when the Tibetan Plateau is 2°C warming.

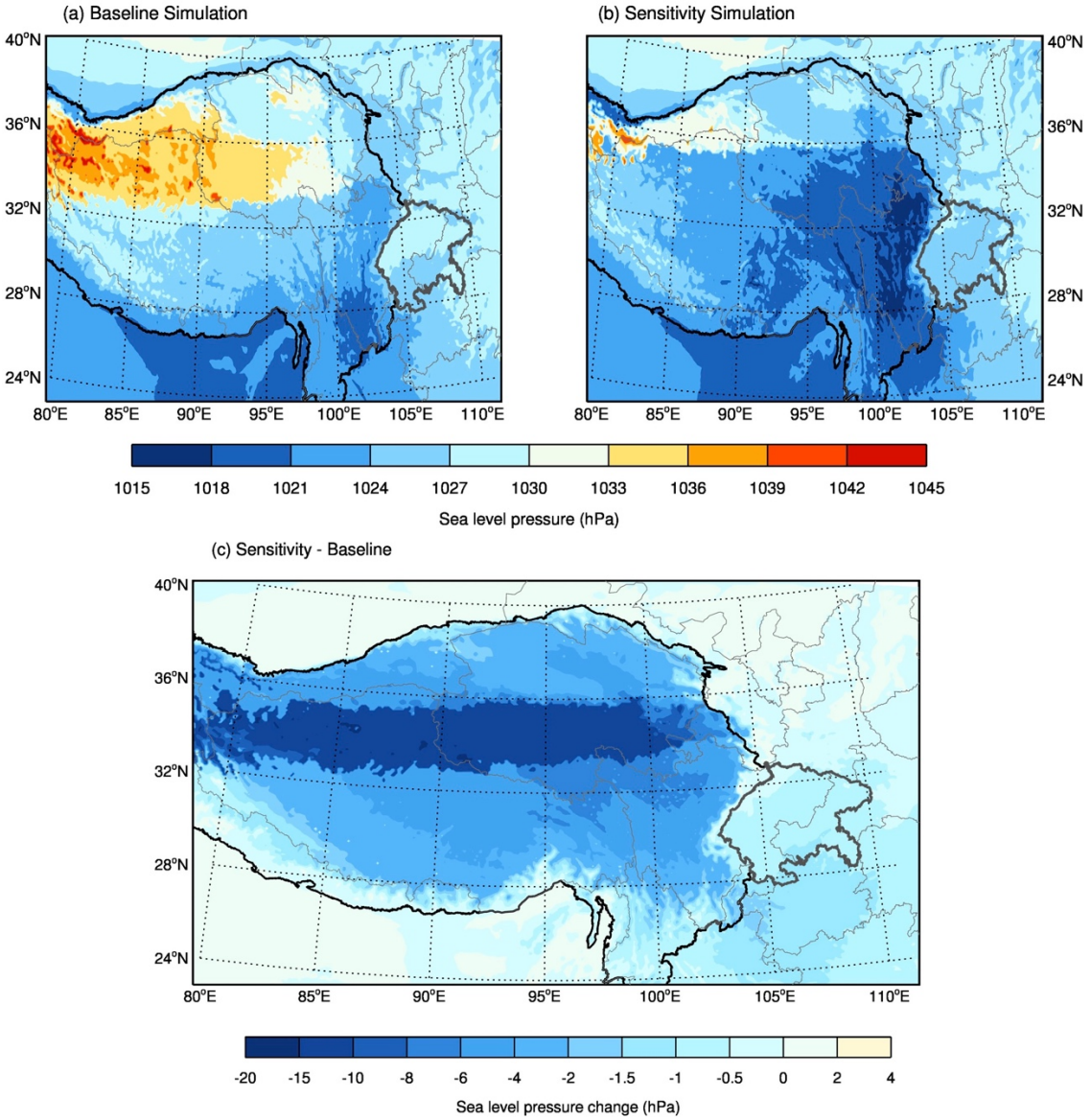


**Figure 8** Comparison of spatial distributions of sea level pressure (SLP) between the (a) baseline simulation and (b) sensitivity simulation over the Tibetan Plateau and Sichuan Basin. (c) The SLPs over the plateau and basin decrease while the plateau becomes 2°C warming.

650

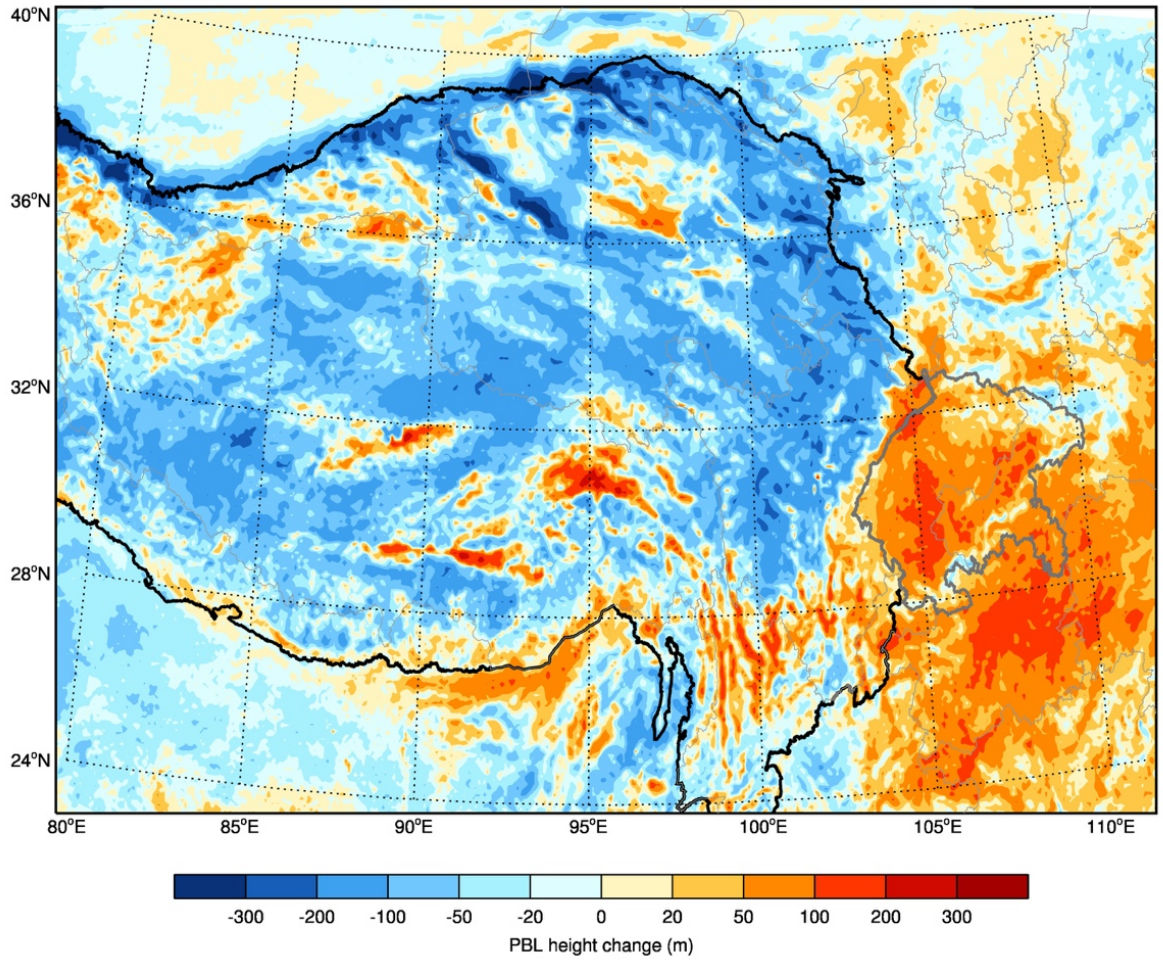


651

652 **Figure 9** Spatial change in the PBL height induced by 2°C warming over the Tibetan Plateau. The positive
653 shows the PBL height increases while the negative shows the PBL height decreases.

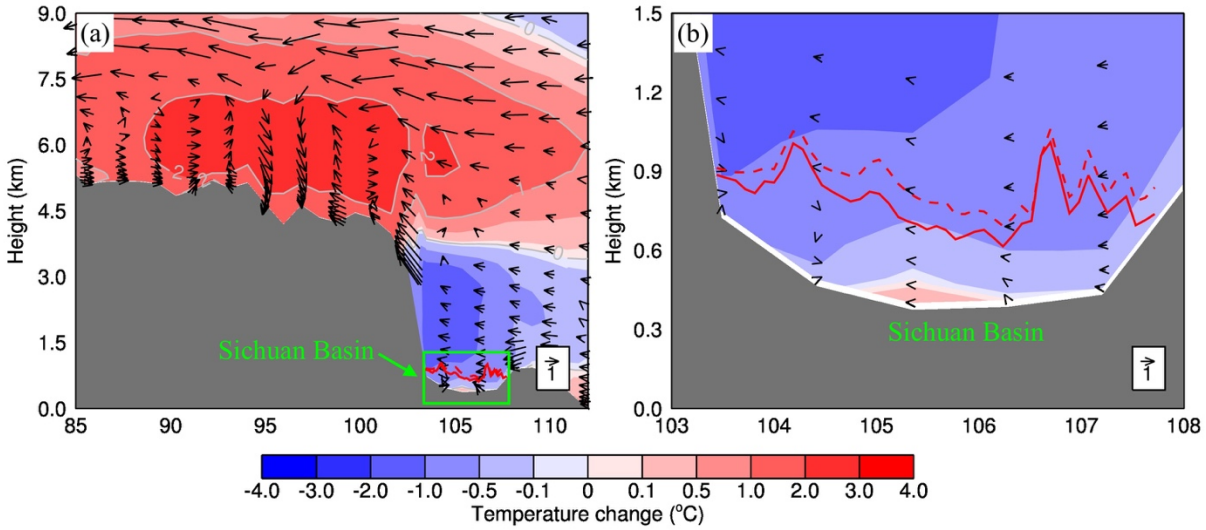


**Figure 10** Vertical profiles of changes in temperature (color shading and gray contour) and winds (arrows) along 30°N in January 2014. The gray shaded area presents topography. The green box for the Sichuan Basin, and the red solid (baseline simulation) and dash (sensitivity simulation) lines for the PBL height. (a) The Tibetan Plateau and Sichuan Basin, and (b) The Sichuan Basin.

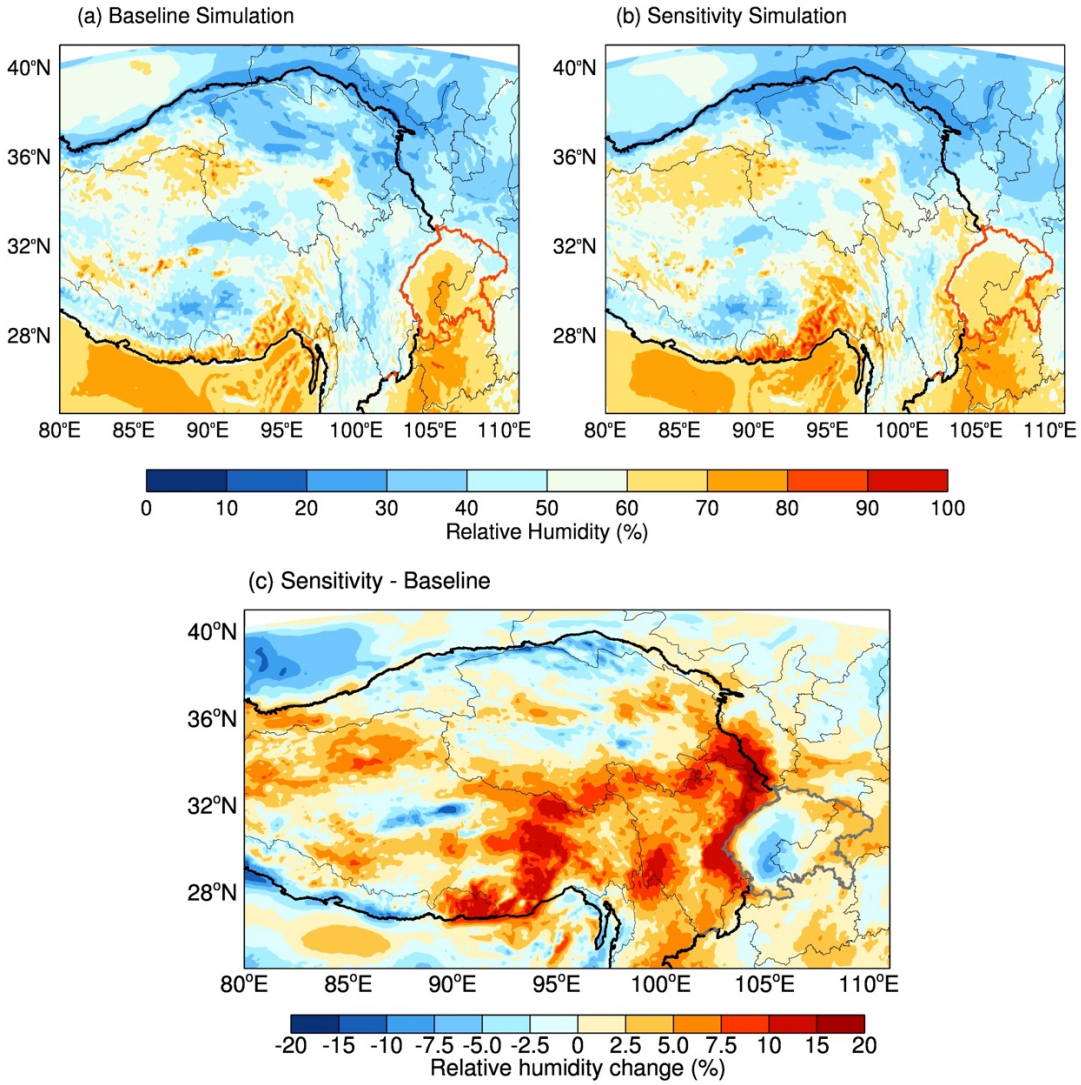


**Figure 11** Comparison of spatial distributions of relative humidity (RH) between the (a) baseline simulation and (b) sensitivity simulation over the Tibetan Plateau and Sichuan Basin. (c) Spatial changes in RH after the plateau becomes 2°C warming, and the positive shows the RH increases while the negative shows the RH decreases.